J. Fluid Mech. (1992), *vol.* 235, *pp.* 123–141
Printed in Great Britain

The unsteady motion of a bubble or drop towards a liquid–liquid interface

By PETER J. SHOPOV AND PETER D. MINEV
Centre for Mathematics and Mechanics, acad. G. Bonchev str. bl. 8, 1113 Sofia,
P.O. Box 373, Bulgaria

(Received 25 September 1990 and in revised form 27 July 1991)

The buoyancy-driven motion of bubbles or drops towards a liquid–liquid interface at small and moderate Reynolds numbers is studied. Solutions of the unsteady nonlinear mathematical problem are performed by means of a general finite-element technique of Lagrangian type. Data for the development of the interface shapes and the film thickness are presented, and comparisons with previous theories and experiments are performed, supporting the reliability of our results. Two interesting phenomena are observed: a transient concavity at the bottom of the particle and particle elongation in the direction of motion. The drainage of the film formed between the particle and the interface, and the tailing mode are studied. Occurrence of a transient surface wave at the liquid–liquid interface and a toroidal dimpling in the film zone are observed in the tailing mode.

1. Introduction

The dynamics of fluid particles rising through an immiscible fluid toward a deformable liquid–liquid interface due to buoyancy is important in several chemical engineering processes. To understand these processes it is useful to study the motion of a single particle moving toward an initially flat fluid–fluid interface. This problem has been studied both experimentally and theoretically under various restrictions in many works, some of which will be briefly reviewed below.

Let fluid 1 contain a bubble or a drop of fluid 2, rising towards the interface between fluids 1 and 3. Three different cases are identified in the literature depending on the properties of the fluids: (i) fluid 2 and fluid 3 are identical (coalescence problem); (ii) the fluids are distinct but miscible; (iii) the fluids are distinct and immiscible.

In general, three steps of this process can be distinguished: (*a*) remote interaction of the particle with the fluid–fluid interface; (*b*) close-range interaction of the particle with the interface. In this stage, a liquid film is formed at the front part of the particle. At large times a tail, due to the deep penetration of the particle into the upper liquid, can appear; (*c*) rupture of the film or the tail, and formation of new structure.

In the present paper we shall consider stages (*a*) and (*b*) of the process for cases (i) and (iii).

The initial stage (*a*) of the process has been studied theoretically only in the context of low-Reynolds-number flow, based on knowledge of the fundamental solution of the Stokes equations and the formulation of the problem in terms of an integral equation. Chi & Leal (1989) studied the initial phase of the coalescence of a deformable drop with a bulk fluid. They restricted their attention to the case of small

inertia (Reynolds number $\mathscr{R} \ll 1$), and examined the influence of the capillary number and viscosity ratio on the interface and drop shapes, as well as on the film profile. The motion of a rigid spherical particle toward an initially flat deformable interface was studied by Geller, Lee & Leal (1986), using the same approach. In recent years, such numerical methods of boundary-integral type have been intensively used in free-surface hydrodynamics and especially in problems connected with deformable particles. They yield many interesting results even for direct study of the particle stability – see e.g. Pozrikidis (1990).

The above-mentioned investigations cover the close-range interaction too but they do not yield theory for the drainage of the hydrodynamical film. This needs development of special methods including coupling of large- and small-scale models (i.e. for the particle and the deformed interface and for the film or tail zone).

The studies of the small-distance interaction are concentrated mainly on the film drainage and only the two interfaces are considered, with some boundary conditions at the film ends, with a fair approach to accuracy. Many theoretical investigations are based on the lubrication theory – Hartland (1969); Riolo, Reed & Hartland (1975); Jones & Wilson (1978). This approach requires knowledge of the initial film shape. Hartland (1969) determines it using experimental observation. Princen (1963) and Jones & Wilson (1978) determine the initial film profile from the static force balance, assuming that the configuration is in a quasi-static equilibrium and neglecting the influence of the film drainage. However, such an equilibrium does not exist in some cases, e.g. when a so-called 'tail' configuration appears, and this assumption is irrelevant. Then the film analysis has to be connected with the overall particle shape and the flow in the other part of the domain.

Many experimental studies are devoted to the motion of a drop toward a fluid–fluid interface and coalescence (MacKay & Mason 1963; Princen & Mason 1965; Hartland 1967*a–c*, 1968, 1969), which is connected with its apparent importance. They provide data for the shape of the drop and the interface, modes and rate of film drainage.

An experimental study of a liquid drop passing through a liquid–liquid interface has been reported by Shan, Wasan & Kintner (1972), where the behaviour of a drop at a pure interface has been compared with that at an impure interface.

In general, the final stage of the interaction of a particle with a fluid–fluid interface is well studied. However, these investigations do not yield the complete picture of the process. The final stage of the interaction of the particle with the interface depends on the earlier stage and these relations are not analysed completely. Usually, the initial film shape is determined from the static force balance, neglecting the inertial and viscous forces. Furthermore, almost all of the preceding theories have analysed film drainage with either zero tangential stress or no-slip conditions at both interfaces of the film. So it is difficult to assess the influence of the physical properties of the fluids beyond the boundaries of the film.

In this study, we present computations for the motion of a fluid particle (bubble or drop) towards a liquid–liquid interface at low and intermediate Reynolds numbers. The Reynolds number is increased until instabilities appear. The numerical solution is based on the unsteady Navier–Stokes equations with force balance boundary conditions on the interfaces, and all transient, nonlinear and free-surface effects are included under no additional restrictions. We assume that the problem is axisymmetric which is consistent provided that the initial condition is axisymmetric. To obtain the solution of this problem we employ a finite-element technique in

conjunction with a Lagrangian approach for the time integration. The numerical method is described in Shopov (1990).

This technique has been successfully used by Shopov *et al.* (1990) for studying the interaction of a gas bubble with a rigid wall. In this paper a large number of test examples and comparisons with the other authors are presented which validate the accuracy of this technique for free-boundary problems. The present work is a continuation of these investigations. Preliminary information about it is included in Minev (1990).

In the present study the shapes of the particle and the interface, as well as the flow pattern, are obtained as a function of time. The film profile and velocity distribution in it are calculated for a small-distance interaction. The influence of the hydrodynamical parameters is studied. Our theory is compared with the results of Chi & Leal (1989) and Hartland (1969) as well as with results of Jones & Wilson (1978) for the film drainage rate. We consider here only interfacial, viscous, inertial and gravitational forces. Our investigations do not concern thin films, and the London–Van der Waals forces are not included in our model. Moreover, the numerical technique is not applicable to the case of coalescence of a gas bubble with a gas bulk phase.

In the next section, the mathematical model is described, with brief information about the procedure for the numerical integration. In the third section the numerical results are presented. The last section contains conclusions drawn from the present study and related discussions.

2. Mathematical formulation and solution methodology

We consider a drop or a bubble of a relatively lighter fluid 2 (i.e. $\rho_2 < \rho_1$) rising through an immiscible ambient fluid 1 under buoyancy toward an initially flat interface (see figure 1) which separates fluid 1 from an upper lighter bulk fluid 3 (i.e. $\rho_1 > \rho_3$). All liquids involved are homogeneous, incompressible, Newtonian, with constant viscosities μ_i and densities ρ_i. Furthermore, the fluid–fluid interfaces are pure and characterized by constant interfacial tensions, denoted by σ_{12} and σ_{13} respectively.

We choose as a reference length the radius of the volume-equivalent sphere

$$l = (3V/4\pi)^{\frac{1}{3}}, \tag{1}$$

where V is the volume of the particle. A characteristic velocity is chosen to be the terminal Stokes velocity U_0 of a rigid sphere of the same density and volume,

$$U_0 = \frac{2(\rho_1 - \rho_2) g l^2}{9\mu_1}, \tag{2}$$

where g is the acceleration due to gravity. The computations show that this is an appropriate choice because the maximum of the actual velocity is indeed $O(1)$. The characteristic time and pressure are respectively U_0/l and $\rho_1 U_0^2$. This reference set yields the following set of dimensionless governing parameters: the Reynolds and Eötvös numbers,

$$\mathscr{R} = \frac{l U_0 \rho_1}{\mu_1}, \quad \mathscr{E} = \frac{g l^2 (\rho_1 - \rho_2)}{\sigma_{12}}; \tag{3}$$

the ratios of the viscosities, surface tensions and densities

$$\lambda_2 = \mu_2/\mu_1, \quad \lambda_3 = \mu_3/\mu_1, \quad \gamma = \sigma_{13}/\sigma_{12}, \quad \delta_2 = \rho_2/\rho_1, \quad \delta_3 = \rho_3/\rho_1; \tag{4}$$

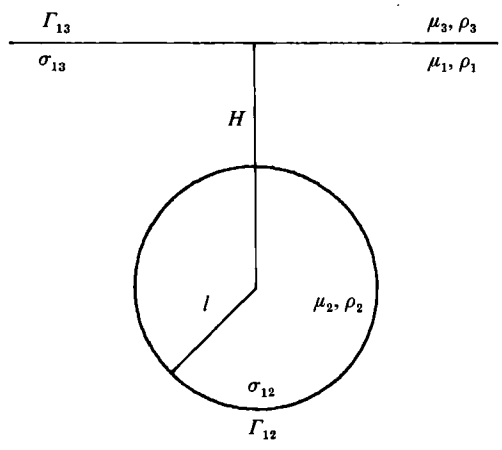

FIGURE 1. Initial configuration of the particle and the interface.

and a geometrical parameter, namely the dimensionless initial distance between the centre of the particle and the interface (see figure 1)

$$d = d(0) = H/l. \tag{5}$$

The Weber, Froude and capillary numbers are functions of the above set of parameters:

$$\mathscr{W} = \frac{\rho_1 U_0^2 l}{\sigma_{12}} = \frac{2\mathscr{R}\mathscr{E}}{9}, \quad \mathscr{F} = \frac{U_0^2 \rho_1}{gl(\rho_1 - \rho_2)} = \frac{2\mathscr{R}}{9}, \quad \mathscr{C} = \frac{U_0 \mu}{\sigma_{12}} = \frac{2\mathscr{E}}{9}. \tag{6}$$

The motion of the ith liquid ($i = 1, 2, 3$) is described by the dimensionless Navier–Stokes equations:

$$\delta_i \left(\frac{\partial \boldsymbol{v}^{(i)}}{\partial t} + (\boldsymbol{v}^{(i)} \cdot \nabla)\, \boldsymbol{v}^{(i)} \right) = \nabla \cdot \boldsymbol{T}^{(i)} + \boldsymbol{F}^{(i)}, \tag{7}$$

$$\nabla \cdot \boldsymbol{v}^{(i)} = 0, \tag{8}$$

$$\boldsymbol{T}^{(i)} = -p^{(i)} \boldsymbol{I} + \frac{\lambda_i}{\mathscr{R}} \boldsymbol{E}^{(i)}, \tag{9}$$

$$E_{kl}^{(i)} = 0.5 \left(\frac{\partial v_k^{(i)}}{\partial x_l} + \frac{\partial v_l^{(i)}}{\partial x_k} \right), \tag{10}$$

where $\boldsymbol{I}$ is the unit tensor, $\boldsymbol{F}^{(i)} = \rho_i \mathscr{F} / (\rho_1 - \rho_2)$ is the vector of the body force, and $\lambda_1 = \delta_1 = 1$.

If the phase i is a gas, the pressure inside this phase depends only on time, i.e.

$$p^{(i)} = p_0(t) \tag{11}$$

The boundary condition at infinity is

$$|\boldsymbol{v}^{(i)}| \to 0 \quad \text{when} \quad |\boldsymbol{x}| \to \infty \tag{12}$$

The kinematic condition at the liquid–liquid interfaces is the continuity of the velocity

$$\boldsymbol{v}^{(i)}|_{\Gamma_{ij}} = \boldsymbol{v}^{(j)}|_{\Gamma_{ij}}. \tag{13}$$

The dynamic condition is:

$$\boldsymbol{T}^{(i)}\boldsymbol{e}_n - \boldsymbol{T}^{(j)}\boldsymbol{e}_n = -\frac{\sigma_{ij}}{\sigma_{12}\mathscr{W}}\left(\frac{1}{R_1}+\frac{1}{R_2}\right)\boldsymbol{e}_n, \tag{14}$$

where σ_{ij} is the surface tension on Γ_{ij}, R_1 and R_2 are the principle radii of curvature of Γ_{ij}, $\boldsymbol{e}_n$ is the outward unit normal to Γ_{ij} for ith phase. If the ith phase is a gas then

$$\boldsymbol{T}^{(i)} = p_0(t)\boldsymbol{I}, \tag{15}$$

If Γ_{ij} is described by the equation $S_{ij}(\boldsymbol{x}, t) = 0$, then the free-surface shape can be determined from the standard kinematic condition:

$$\frac{\mathrm{D}S_{ij}(\boldsymbol{x}, t)}{\mathrm{D}t} = 0. \tag{16}$$

There are many possibilities for the choice of the initial conditions for this problem. Usually the particle is assumed to be spherical and at rest in quiescent liquid and the interface to be flat at the initial instant. This is a natural initial condition but is often violated in practice. So we also consider numerical examples with two other initial conditions: an elongated particle at rest, and the steady-state shape and the velocity field for the same particle in unbounded ambient liquid – see Dandy & Leal (1989).

A general finite-element technique of Shopov (1990) is used to solve this problem, see also Bach & Villadsen (1984), Keunings (1986). The finite elements are isoparametric with a 9-node quadratic approximation for the velocity and a linear approximation for the pressure – see Engelman *et al.* (1982). As the equations are unsteady, the Lagrangian approach is used for time integration. The mesh cells represent finite volumes of the liquid moving with the flow. When they become intolerably stretched, a regridding is performed. A general procedure of grid redefinition is developed which allows us to change the number of finite elements, as well as the topology of the mesh.

To compute the evolution of the fluid–fluid boundaries, a predictor-corrector procedure is used. In order to minimize the computational time an adaptive method for automatic adjustment of the time step is developed. We require that the maximum of the difference between the predicted and corrected position of the interfaces at each time step is less than a pre-established maximum. If this criterion is satisfied the time increment can be increased; if not, we decrease it and repeat the current step. A gross measure ϵ for the accuracy is taken usually to be about 1 % of the unit length multiplied by the actual time integration step. So if this accuracy cannot be assured, then the time integration stops. This is why the method is unable to give information for the last stage of close-range interaction: because of the mesh degeneration in the film zone. We incorporate in our numerical scheme a spline procedure for filtrating the error in the computed values of the velocity of the interfaces. More information about the numerical technique can be found in Shopov (1990).

A number of tests and comparisons with other theoretical and experimental results for free-boundary problems are presented in Shopov *et al.* (1990), with reliability tests of this method included. In order to provide further corroborative results we present in §3 a direct comparison with the study of Chi & Leal (1989) of the slow motion of a drop towards a liquid–liquid interface, which is based on a boundary-integral method.

Good adaptivity of this method to different problems is its virtue, as well as the possibility of considering many liquids and interfaces. This is possible due to the usage of a discontinuous pressure approximation, which also yields very good results for flows in fixed domains – see e.g. Cliffe & Lever (1986). The method works well for problems in which the particle rims are quite sharp as presented in figures 5 and 7. This seems to be more difficult for the methods based on a transformation of the physical domain to a fixed computational one – see e.g. Dandy & Leal (1989).

3. Results

As mentioned in the introduction, we focus our attention on the intermediate- and small-distance interaction stages but only for relatively large film thickness. The solution procedure does not work very well when the film becomes very thin. Then the lengthscales inside and outside the film are too different and so, to achieve a good accuracy in the both regions, a large number of finite elements is required which is not possible because of the capabilities of the computers we have used. The lowest film thickness attained in our experiments is about 0.011 with respect to the particle equivalent radius (1). Chi & Leal (1989) met with similar difficulties and stopped their computations when the thickness of the film became less than 0.02 of the undeformed particle radius.

3.1. *Bubble approaching a liquid–liquid interface*

In this case fluid 2 is a gas and the system (7)–(10) is reduced to equations for liquids 1 and 3 only. Then for convenience we take $\lambda = \lambda_3$ and $\delta = \delta_3$.

First, we consider a bubble rising under buoyancy to a deformable interface at intermediate Reynolds number, $\mathscr{R} = 2$. The starting distance is moderate, $d = 1.5$, and the interaction of the bubble with the interface begins before it achieves its terminal velocity in an unbounded liquid. Bubble flattening and interface bulging develop as a result of the interaction, see figure 2. At the last instant presented in figure 2 the interfaces are close to a quasi-static equilibrium. The film between them drains uniformly and the calculations are stopped when its thickness reach 0.015 of the undeformed bubble radius. The shape of the film is hemispherical with dimensionless radius of curvature about 1.1. The angle θ between the axis of symmetry and the line connecting the centre of curvature and the edge of the film is about 70°. Since the inertial effects are moderate, a qualitative comparison with the low-Reynolds-number theory of Chi & Leal (1989) is appropriate. In all their results at $\lambda = 0.1$ a 'rapid drainage' occurs and the film thickness increases monotonically as r increases. In the present case $\lambda = 0.333$ and the profile is uniform. However, the rate of drainage is relatively high in comparison with the numerical examples with larger viscosity ratio λ – see figure 8. A ln–ln plot of the film thickness at the centreline, H_{cen}, as a function of t is presented in figure 3 (a). The film-drainage analysis of Jones & Wilson (1978) predicts that the film thickness should decrease asymptotically at a rate proportional to $t^{-\frac{1}{3}}$ for a film between two free surfaces. In order to compare our result with this theory we evaluate numerically the derivative $\mathrm{d}(\ln H_{\text{cen}}(\ln t))/\mathrm{d}(\ln t)$ in the time interval $4.25 < t < 5.12$ (the calculations are stopped at $t = 5.12$). Its value is 0.3, which differs by about 10% from the asymptotic prediction of Jones & Wilson. So we can expect a good asymptotic agreement of the rate of drainage. However, we cannot make a stronger statement from the numerical data available.

In this case, as well as in most of the computations presented below, we assume

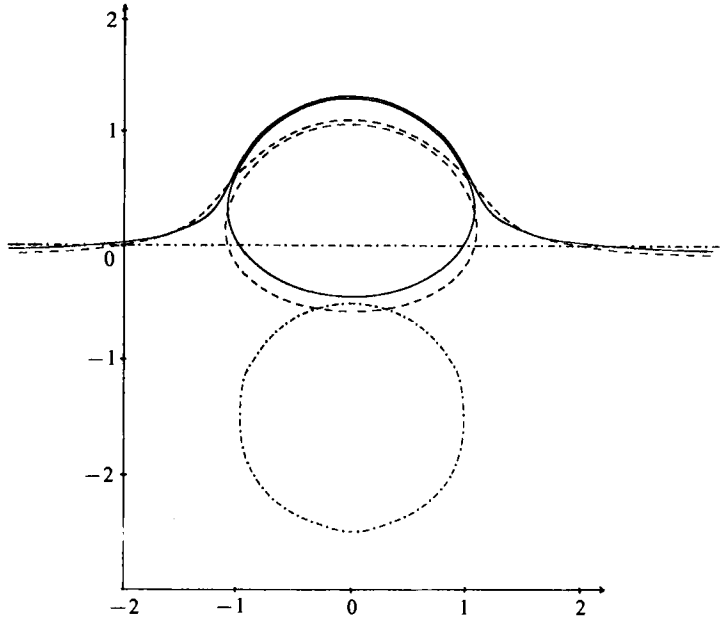

FIGURE 2. Bubble rising towards a liquid–liquid interface, $\mathscr{R} = 2$, $\mathscr{E} = 2$, $\lambda = 0.333$, $\gamma = 0.4$, $\delta = 0.2$, $d = 1.5$: -·-·-·-, $t = 0$; – – –, $t = 2.8$; ——, $t = 5.1$.

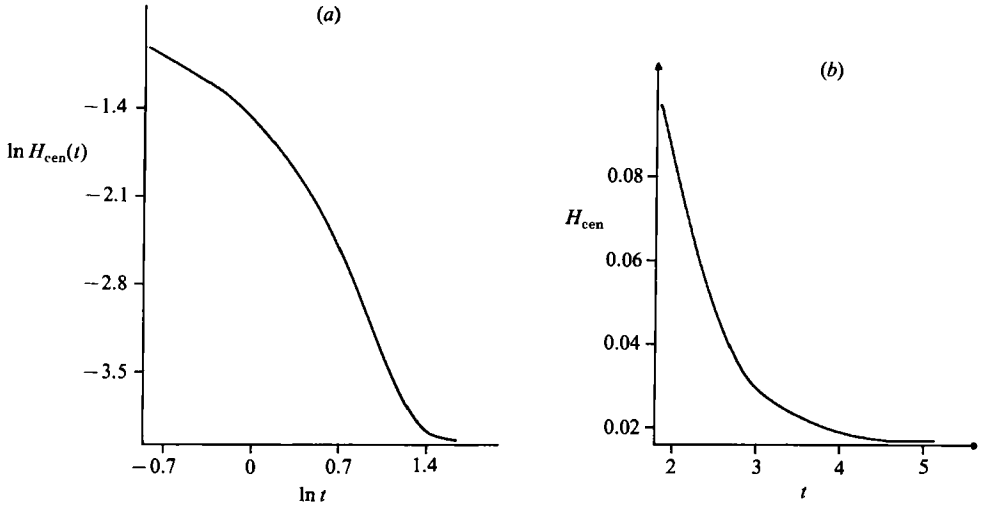

FIGURE 3. Graph of dimensionless film thickness at the centreline: (*a*) $\ln H_{cen}$, (*b*) H_{cen} for the experiment in figure 2.

that the particle is released from a nozzle close to the bulk interface and its initial shape is spherical. The last assumption is reasonable for most low-Morton-number systems, but can be significantly in error if $\mathscr{M}$ is large (see Clift, Grace & Weber 1978). In such a case the initial shape of the particle is usually elongated. In order to verify the dependence of our results on the initial shape of the particle we carry out computations with an initially elongated bubble at the same parameters as in the case discussed above. The evolution of the interfaces is presented in figure 4. As one

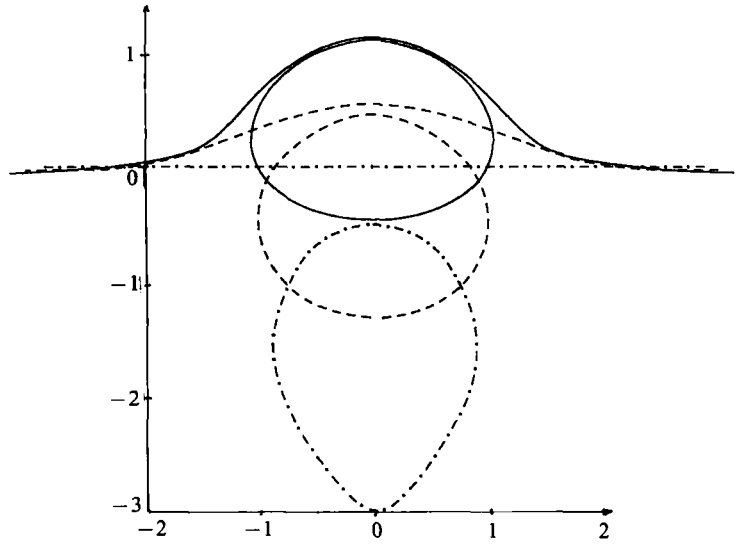

FIGURE 4. Bubble rising towards a liquid–liquid interface, $\mathscr{R} = 2$, $\mathscr{E} = 2$, $\lambda = 0.333$, $\gamma = 0.4$, $\delta = 0.2$, $d = 1.5$, elongated initial shape: –·–·–, $t = 0$; – – –, $t = 1.6$; ——, $t = 3.3$.

can see the bubble deforms fast under the action of surface tension and inertia and for $t \approx 0.7$ it is nearly spherical. For $t > 1$ the interface shapes in both cases are nearly the same. The quasi-static state and the film profile also do not differ significantly.

Hence the variation in the initial shape of the particle influences the process only for a small time period, and results obtained under the assumption of a spherical initial particle shape can be also used in other cases.

Next, we consider a case where the upper liquid is considerably less viscous than the bulk one. In this case a new hydrodynamic effect takes place – the elongation of the bubble in the close-range interaction phase of the process, see figure 5. To show this effect in a clear form we present here an experiment for small Reynolds and Weber numbers, $\mathscr{R} = 0.039$; $\mathscr{W} = 0.0275$. It is well known that for these values of the governing parameters the bubble remains spherical in unbounded liquid (see the experiments of Bhaga & Weber 1981, the theory of Taylor & Acrivos 1964 and numerical experiments of Shopov *et al.* 1990) and any variation in shape is purely due to the presence of the interface.

The evolution of both interfaces in the case where the upper liquid is a hundred times less viscous than the bulk one is shown in figure 5. As expected, the bubble remains spherical for small times (i.e. about $t < 0.1$). The interaction of the particle with the interface begins when the distance between them is comparatively large, $d(t) = 1.49, t = 0.01$. One reason is the well known fact that the zone of the disturbance in front of the particle is larger for greater viscosity. The small surface tension on the liquid–liquid interface and the low viscosity of the upper liquid result in resistance at the front part of the particle that is lower than that at its rear remaining in the viscous bulk. Hence, when the particle approaches the interface, gravity dominates the dynamics of the front part; the viscous tension is dominant at the rear, causing its lag. Although the deformability of the gas–liquid interface is small ($\mathscr{E} = 2.13$; $\mathscr{W} = 0.0275$), the elongation of the particle in the direction of the motion is considerable and reaches 25 % at the end of the simulation presented in figure 5. The velocity of the fore point of the particle is steadily greater than the velocity of the

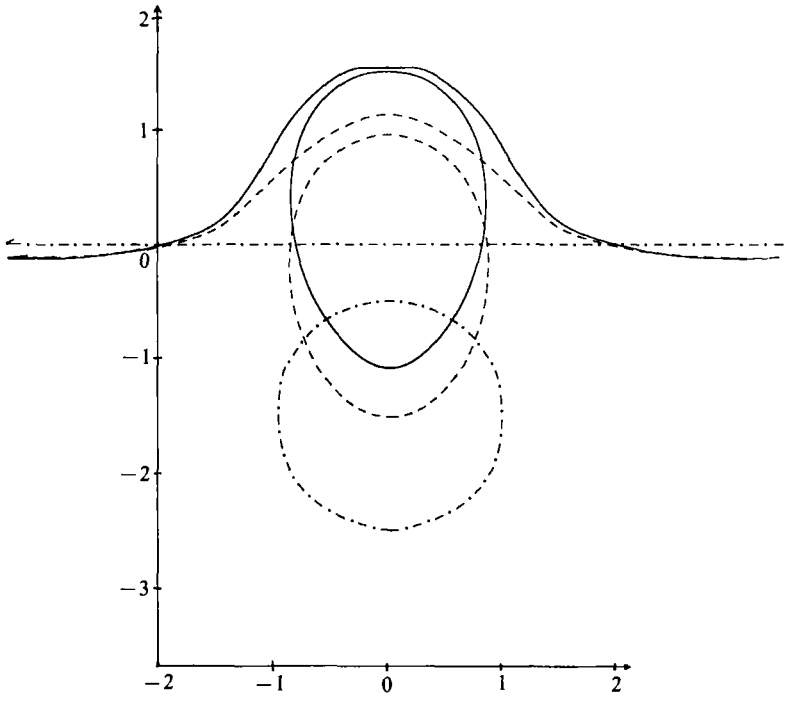

FIGURE 5. Motion of a bubble towards a liquid–liquid interface, $\mathscr{R} = 0.039$, $\mathscr{E} = 2.16$, $\lambda = 0.0039$, $\gamma = 0.00275$, $\delta = 0.9$, $d = 1.5$: –·–·–·–, $t = 0.01$; – – –, $t = 1.2$; ——, $t = 1.6$.

rear one (e.g. for the last shape in figure 5 the ratio between them is 2.6). A similar effect of particle elongation was observed in the experiment of Shan *et al.* (1972) when a water drop passes through an interface between DC 200 and cyclohexanol.

The film drainage mode is 'rapid'. Chi & Leal (1989) have predicted such a film profile in the case of coalescence of a drop at low $\mathscr{R}$ if $\lambda \leqslant 1$. In our case one of the film interfaces is free (zero tangential stress), and $\lambda = 0.0039$ which means that tangential stress on the other one is very small. So the rapid drainage is in agreement with the prediction of Chi & Leal. The calculations are stopped when the film thickness H_{cen} is about 0.012. The penetration of the particle into the upper liquid is now much deeper than in the previous case owing to the considerably higher deformability of the liquid–liquid interface. For the same reason, the final shape is far from being quasi-static, but we have to stop the simulation because of the small thickness of the film.

In order to study the influence of the initial velocity field, another experiment is carried out at the same parameters, but with a different initial condition for the velocity. The bubble terminal shape in an unbounded liquid (it is spherical in this case) and the corresponding velocity field are used as initial conditions, which corresponds to the case of large starting distance d. These conditions are prescribed when the particle is three equivalent radii away from the interface. The consistency of this is supported by the fact that the bubble shape remains unchanged for small times – see figure 6. The effect of elongation is preserved and is more clearly seen, as compared to the previous experiment with moderate starting distance. The elongation of the bubble at the last instant in figure 6 is about 50% of the undeformed bubble radius. The penetration of the particle in this case is greater than

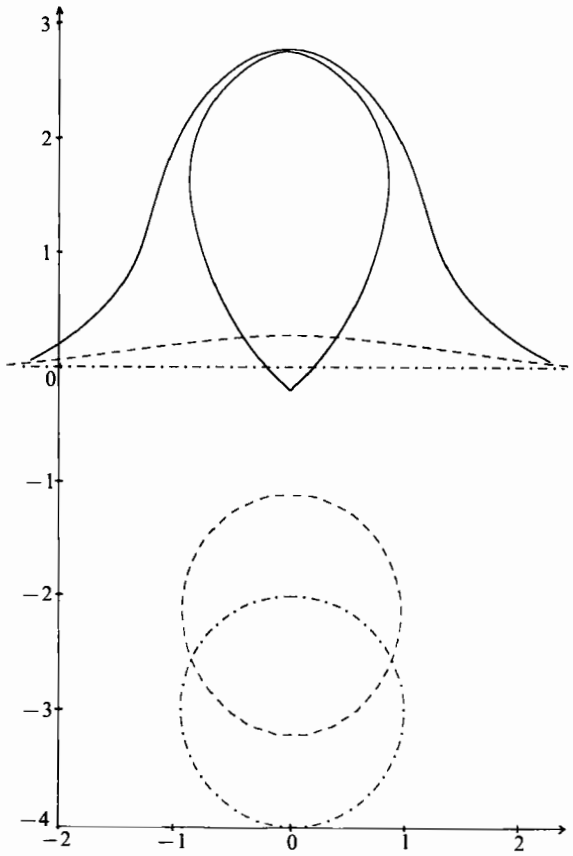

FIGURE 6. Interaction of a bubble at terminal velocity for unbounded liquid with the liquid–liquid interface, $\mathscr{R} = 0.039$, $\mathscr{E} = 2.16$, $\lambda = 0.0039$, $\gamma = 0.00275$, $\delta = 0.9$, $d = 1.5$: –·–·–, $t = 0$; – – –, $t = 2.7$; ——, $t = 4.6$.

in the previous one, owing to the considerable inertia of the particle. At $t \approx 4$ its rear edge begin to sharpen. A similar effect was observed in the experiment of Shan *et al.* (1978) mentioned above.

In order to outline the possible inertial effects in this problem, we present in figure 7 a numerical simulation at a larger Reynolds number, $\mathscr{R} = 60$, while preserving the starting distance the same as that in experiments, given in figures 4 and 5. In addition, we take the upper liquid to be more viscous than the bulk one, $\lambda = 3$, in order to study the influence of this important parameter on the film shape. The deformability of both interfaces is quite high, $\mathscr{W} = 260$, $\mathscr{E} = 20$, and the same, i.e. $\gamma = 1$. The densities ratio is moderate; $\delta = 0.5$, i.e. the bulk liquid is two times heavier than the upper one.

Initially, up to $t = 1.6$ ($H_{\text{cen}} = 0.4$) the bubble retains its spherical shape, which is much longer than in the previously presented cases. It corroborates our argument that the size of the zone in front of the particle where the liquid is disturbed decreases with increasing the Reynolds number.

When the interaction between the bubble and the interface becomes strong (in this case when $t > 3$; $H_{\text{cen}} < 0.32$), an inertial concavity in the rear of the bubble appears. This is due both to the action of the inertial force of the liquid behind the bubble and the resistance of the liquid–liquid interface. This effect was observed by Shopov *et al.*

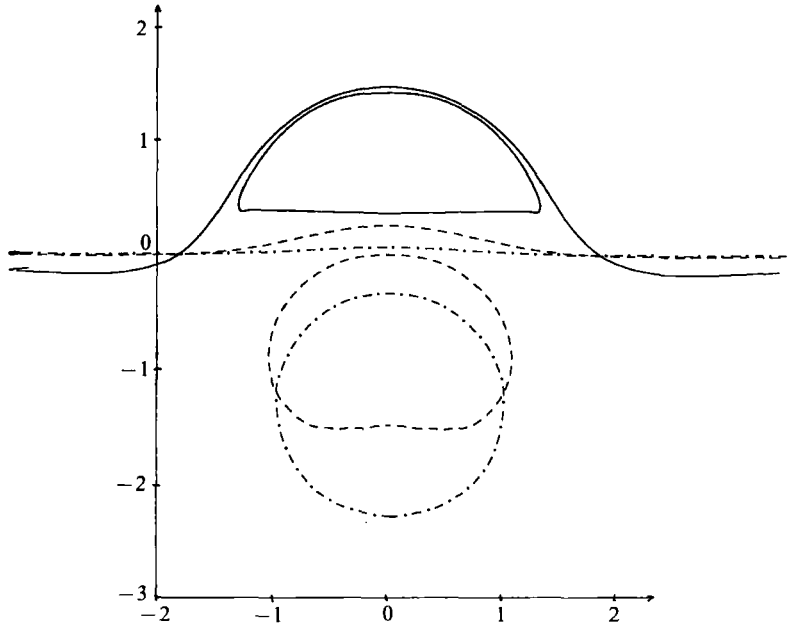

FIGURE 7. Motion of a bubble towards a liquid–liquid interface, $\mathscr{R} = 60$, $\mathscr{E} = 19.5$, $\lambda = 3$, $\gamma = 1$, $\delta = 0.5$, $d = 1.5$: –·–·–, $t = 1.6$; – – –, $t = 3.6$; ——, $t = 15.5$.

(1990) for the same problem but with a liquid–rigid wall interface. At the same time, considerable overall flattening of the particle and bulging of the liquid–liquid interface take place, as in the first experiment presented.

After a time (approximately for $t > 5$) the surface tension at the rear becomes dominant. It acts to reduce the concavity and thus causes a surface wave, which can be observed in the last two shapes on figure 7. The wave amplitude decreases quickly and at $t = 15.5$ the shape configuration is nearly quasi-static. At $t \approx 11$ a dimple is formed at the fore part of the bubble. Its amplitude is modest but it is clearly seen in the numerical data and can be observed at the last shape in figure 7. This effect is due to the higher viscosity of fluid 3 (see figure 1), which results in the growth of the tangential stress on Γ_{13} with respect to the two previous examples. This behaviour is again in agreement with the theory of Chi & Leal (1989), which predicts the occurrence of the dimpling if $\lambda \gg 1$. Their results are obtained for the quasi-static, Stokes flow case. It is interesting to note that the viscosity ratio remains the most important factor for the dimpling formation for intermediate Reynolds numbers also. Of course, the influence of the particle velocity at the moment of film formation is also important (see Shopov *et al.* 1990), and in the case considered the presence of inertial terms contributes to the dimpling formation as well.

Comparisons with the results of Shopov *et al.* (1990) for the same problem but with liquid–rigid wall interface show that, apparently, the dimpling effect is less strong for liquid–liquid interfaces. In the latter case, the film shapes are significantly closer to hemispherical and the film thickness always grows in the region near its ends. If dimpling is present, then the point where the film thickness is minimal is located much nearer to the central line than in case of interaction with a rigid interface.

As we expected, the average rate of 'dimple' drainage in this experiment is lower than the rate of uniform drainage, comparing the graphics of the film thickness in figures 3(*b*) and 8.

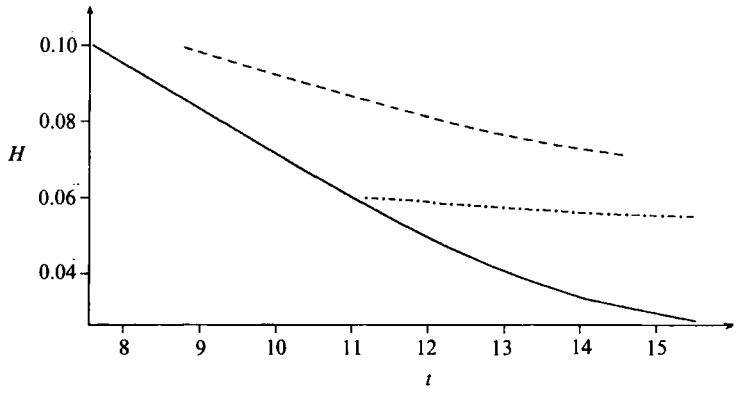

FIGURE 8. Dimensionless film thickness at the centreline $H_{cen}(t)$ (——) and at the rims $H_{min}(t)$ (–·–·–·–) for $\mathscr{R} = 60$, $\mathscr{E} = 19.5$, $\lambda = 3$ (bubble towards a liquid–liquid interface); – – –, $H_{cen}(t)$ for $\mathscr{R} = 2$, $\mathscr{E} = 5$, $\lambda = 0.33$ (coalescence of a drop).

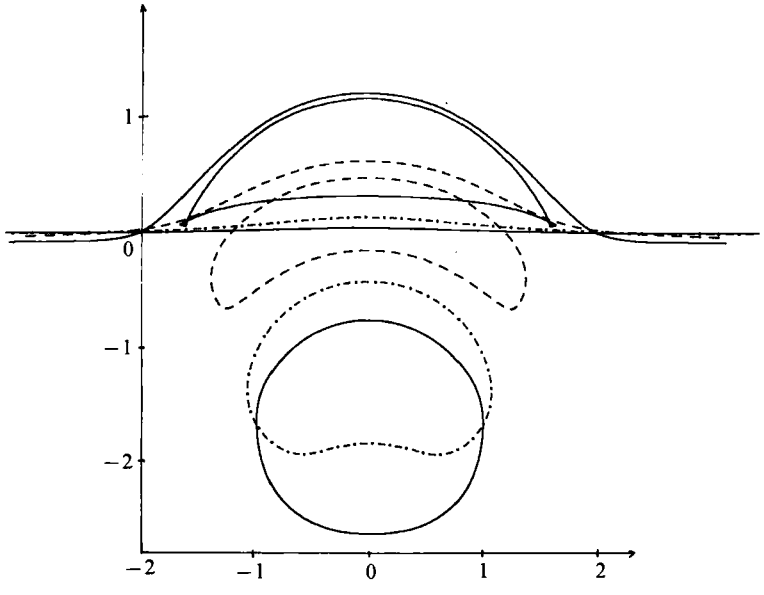

FIGURE 9. Motion of a bubble towards a liquid–liquid interface, $\mathscr{R} = 88$, $\mathscr{E} = 19.8$, $\lambda = 2$, $\gamma = 20$, $\delta = 0.5$, $d = 1.5$: ——, $t = 2.4$; –·–·–, $t = 4.4$; – – –, $t = 10.8$; ——, $t = 17.1$.

Another effect presented at large Eötvös and Reynolds numbers is the sharpening of the rims of the bubble in the small-distance interaction stage. It can be observed for the motion of a bubble in a spherical container (see Shopov *et al.* 1990), where the film shape is again hemispherical.

Finally, in figure 9 we present computations performed to give an idea of when an instability of the bubble surface due to interaction with the interface takes place. The Reynolds and Weber numbers are relatively large: $\mathscr{R} = 88$, $\mathscr{W} = 387$ ($\mathscr{E} = 20$). The inertial concavity at the bubble rear is much greater now, see figures 7 and 9. The surface wave, which develops under the action of the surface tension, causes an instability on the bubble boundary. In the numerical experiment this yields self-crossing of the free boundary, which can be observed in the last position on figure 9. A related situation is observed in experiments mentioned by Harlow & Shannon

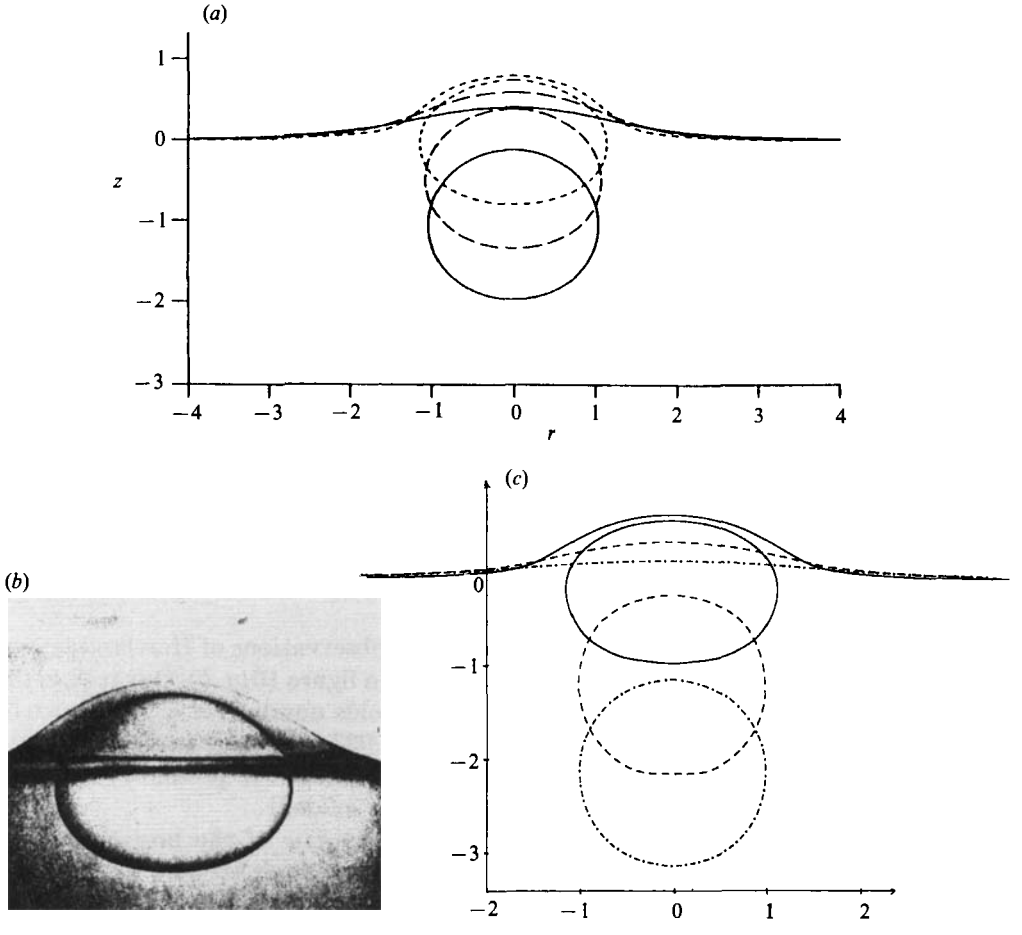

FIGURE 10. Comparison of the results for the motion of a drop towards a liquid–liquid interface: (*a*) Chi & Leal (1989), $\mathscr{G} = 1.0$, $\lambda = 0.02$; (*b*) Hartland (1969), $\mathscr{G} = 1.037$, $\lambda = 0.021$; (*c*) present results for $\mathscr{R} = 0.0021$, $\mathscr{E} = 3.14$, $\lambda = 0.021$, $\gamma = 1$, $\delta = 0.5$, $d = 3$: –·–·–, $t = 1.2$; – – –, $t = 2.3$; ——, $t = 5.1$.

(1967) in the case of a liquid drop interacting with a gas–liquid surface in gas bulk. On the photographs the inertial indentation is very clearly visible and the drop rim sharpens, owing to the interaction with the interface. Naturally, at the last moment an instability in the angular direction develops and small drops separate from the particle. This process is fully three-dimensional, and is not included in our axisymmetric simulation.

3.2. *A drop approaching a liquid–liquid interface*

First, we shall consider the case of coalescence, for which a connection between the governing parameters holds:

$$\lambda = \lambda_1 = \lambda_2, \quad \delta = \delta_1 = \delta_2, \quad \gamma = 1. \tag{17}$$

For this case the low-Reynolds-number theory of Chi & Leal (1989) applies and we shall compare our computations with it. Chi & Leal have employed a quasi-steady approach, which permits to the shapes of the liquid–liquid interfaces to be followed in terms of the distance between them. They present a comparison of the numerical

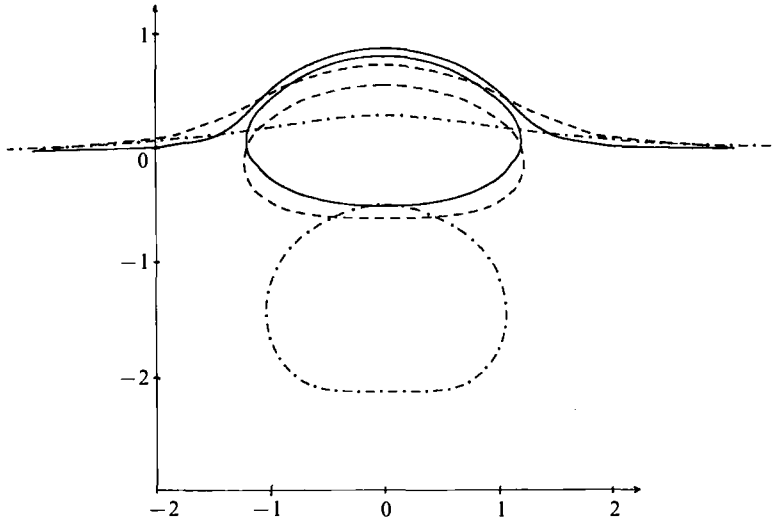

FIGURE 11. Motion of a drop towards a liquid–liquid interface (coalescence), $\mathscr{R} = 2$, $\mathscr{E} = 5$, $\lambda = 0.333$, $\gamma = 1$, $\delta = 0.2$, $d = 1.5$: –·–·–, $t = 2.5$; – – –, $t = 5.9$; ——, $t = 14.7$.

shapes for $\mathscr{C} = 1$ and $\lambda = 0.02$ with the experimental observations of Hartland (1969) for $\mathscr{C} = 1.037$, $\lambda = 0.021$ and these results are shown in figure 10(*a*, *b*). Our results for the evolution of the interface shapes at a small Reynolds number ($\mathscr{R} = 0.1$), $\delta = 0.5$, and the same values of the capillary number $\mathscr{C} = 1.037$, viscosity ratio $\lambda = 0.021$, and the body force parameter (see Chi & Leal) $Cg = 0.00069$ are presented in figure 10(*c*). The qualitative coincidence of all the results is evident.

A measure for quantitative comparison is the ratio h/w of the horizontal and vertical size of the terminal, quasi-static shape of the particle. It is equal to 1.5 in the results of Chi & Leal (1989) and in ours. In the experiment of Hartland (1969) $h/w = 1.3$. The film in all the three results is of uniform thickness. The quasi-static equilibrium is reached in our experiment for $t = 5.8$.

In order to investigate the influence of the internal circulation in the drop on the film drainage, calculations (see figure 11) are carried out for coalescence of the same two liquids as in the experiment with a bubble in figure 2. For a bubble the viscosity ratio $\lambda_2 = 0$, but now the fluid inside the drop is identical with the lighter bulk fluid 3 with $\lambda = \frac{1}{3}$. The other parameters are kept fixed: $\mathscr{R} = 2$, $\mathscr{W} = 2.2$, $\delta = 0.2$, $d = 1.5$, which means that the Eötvös number on the particle–liquid interface is larger now. Because of this the particle in figure 11 appears to be more deformed now in comparison with case in figure 2.

The film drains uniformly. Its shape is hemispherical and in the final moment presented its radius is 1.5 and angle θ (see §3.1) is about 45°. The graph of the film thickness $H_{\mathrm{cen}}(t)$ is shown in figure 8. It decreases linearly up to $t \approx 13.2$ and its slope is approximately 7.5°. For $t > 13.2$ the slope is smaller. In comparison with the graph in figure 3(*b*) the film thickness $H_{\mathrm{cen}}(t)$ decreases more slowly. So we can conclude that the increase of the viscosity ratio and hence of the tangential stress at one side of the film strongly decreases the rate of drainage.

In order to study the influence of the Reynolds and Eötvös numbers on the process of coalescence two experiments are carried out. First we fix $\mathscr{R} = 2$, $\lambda = 0.333$ and $\delta = 0.2$ as the previous experiment and increase the Eötvös number to $\mathscr{E} = 20$. The evolution of the fluid–fluid interface is shown in figure 12. As in the case of a fluid

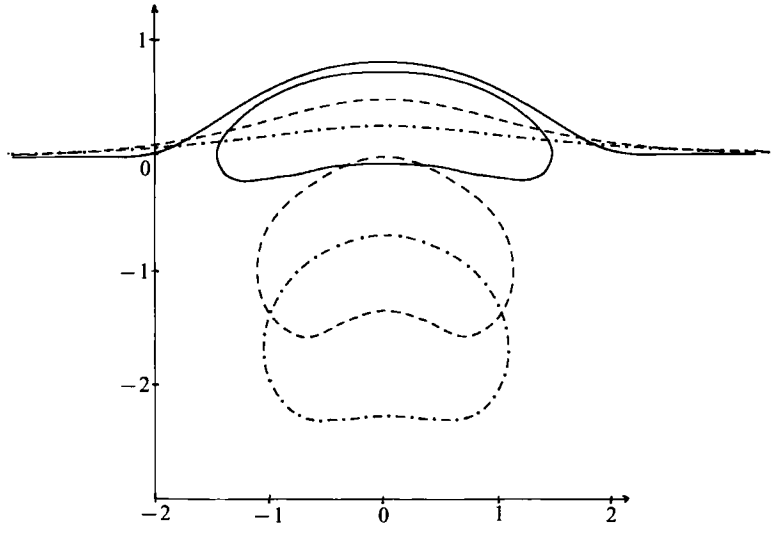

FIGURE 12. Motion of a drop towards a liquid–liquid interface (coalescence), $\mathscr{R} = 2$, $\mathscr{E} = 20$, $\lambda = 0.333$, $\gamma = 1$, $\delta = 0.2$, $d = 1.5$: –·–·–, $t = 2.3$; – – – –, $t = 3.25$; ——, $t = 7.9$.

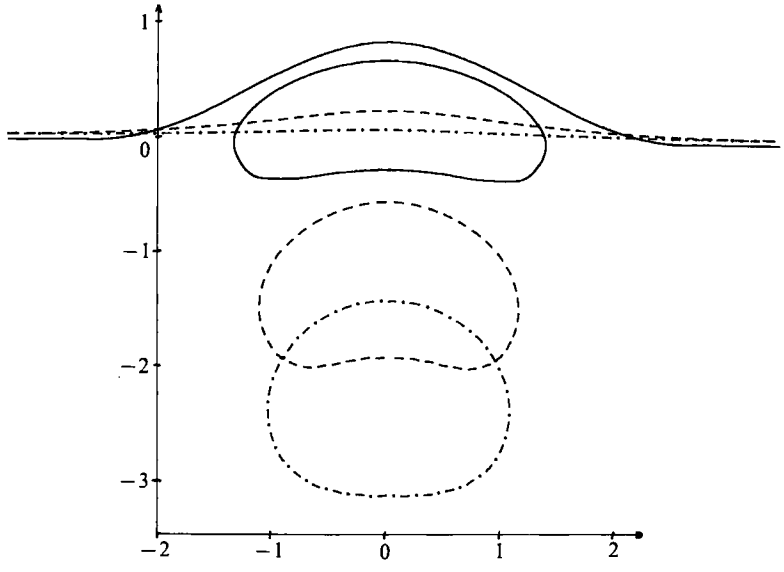

FIGURE 13. Motion of a drop towards a liquid–liquid interface (coalescence), $\mathscr{R} = 10$, $\mathscr{E} = 5$, $\lambda = 0.333$, $\gamma = 1$, $\delta = 0.2$, $d = 1.5$: –·–·–, $t = 1$; – – – –, $t = 3.1$; ——, $t = 7.6$.

particle rising toward a rigid wall (see Shopov *et al.* 1990) the increase of $\mathscr{E}$ leads to an increase of deformation of the particle. The surface tension is 5 times smaller than in the previous case and the inertial forces at the rear of the drop become dominant. They cause a considerable indentation in this zone.

A similar situation takes place if we fix the values of $\mathscr{E} = 5$, $\lambda = 0.333$, $\delta = 0.2$ and increase the Reynolds number to $\mathscr{R} = 10$ (see figure 13). Then the surface tension is not increased but the inertial forces are greater and thus they again cause an indentation in the rear of the particle. However, the profile of the film is not

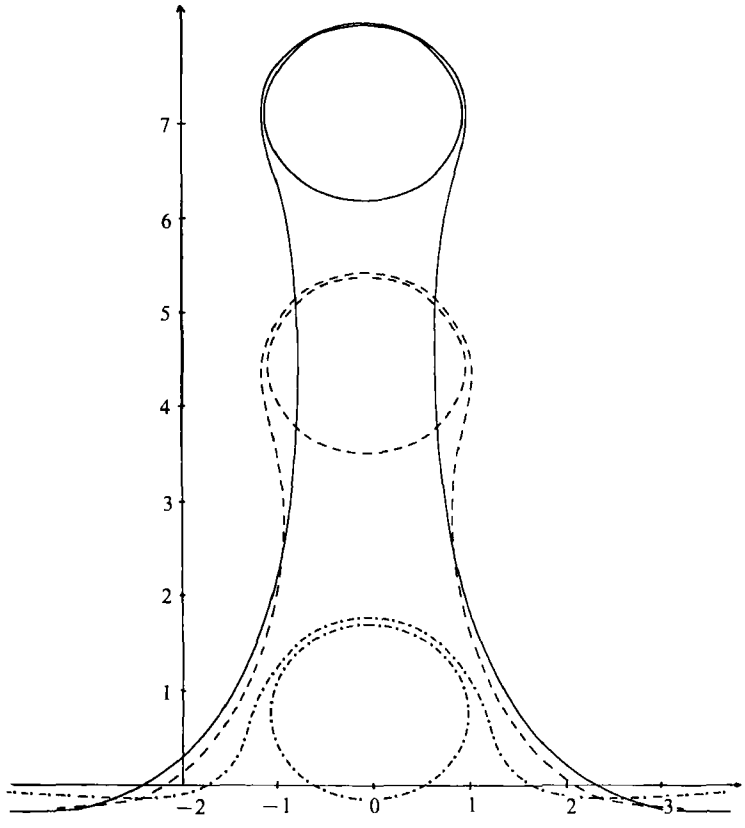

FIGURE 14. Motion of a drop towards a liquid–liquid interface, $\mathscr{R} = 18$, $\mathscr{E} = 1$, $\lambda_2 = 36$, $\lambda_3 = 0.33$, $\gamma = 0.01$, $\delta_2 = 0.1$, $\delta_3 = 0.9$, $d = 3$: –·–·–, $t = 13.68$; – – –, $t = 21.18$; ——, $t = 25.63$.

influenced by these two parameters and the film drains uniformly in both cases, as in the case shown in figure 11. These facts confirm that the most important parameter with respect to the film drainage is viscosity ratio λ.

The so-called 'tailing configuration' cannot occur in coalescence because the density of the particle bulk and of the upper liquid is the same. It would be possible if the three fluids were different and the density of the particle bulk were significantly lighter than that of the upper one.

So we now turn our attention to this situation, taking the drop bulk to be ten times lighter than the ambient liquid, $\delta_2 = \frac{1}{10}$, and nine times lighter than the upper one, $\delta_3 = \frac{9}{10}$. The deformability of the particle interface is modest, $\mathscr{W} = 4$, $\mathscr{E} = 1$, but $\gamma = 0.01$ and so the liquid–liquid interface is easily deformable. In this way the penetration of the particle through the interface is promoted. The ambient liquid is chosen to be not very viscous, $\mathscr{R} = 18$, in order to permit the easy motion of the particle through it, and the upper one is taken to be three times less viscous, $\lambda_3 = 0.33$, for similar reasons. The liquid inside the particle is much more viscous than the ambient one, $\lambda_2 = 36$ and its Reynolds number is 0.5. The starting distance is relatively large, $d = 3$, which allows the particle to gain enough velocity before the start of the interaction with the interface.

As the Archimedean force is dominant, the drop penetrates into the upper liquid, deforming the interface and carrying with it a portion of liquid 1, see figure 14. The rate of film drainage is relatively slow owing to the high viscosity of the particle

liquid, and the displacement of the particle into the upper liquid is about 8.5 equivalent radii.

Similar tailing configurations are observed in the theoretical results of Geller *et al.* (1986) for low-Reynolds-number interaction of a rigid sphere with a liquid–liquid interface and in the experiment of Shan *et al.* (1972) for a water drop passing through the interface between cyclohexanol and DC 200. Both experiments are in good qualitative agreement with our result. Unfortunately the experiment of Shan *et al.* (1972) cannot be used for a quantitative comparison because the interface is very impure and we are unable to obtain values for the governing parameters.

The particle shape remains nearly spherical until the small-distance interaction phase, when a slight flattening takes place. Its maximum is achieved at the moment when the particle begins to move the interface up. It is due to the reaction of the surface tension at the liquid–liquid interface.

A surface wave is observed at the liquid–liquid interface at the moment of one-diameter penetration of the particle into the upper liquid. This effect is not purely viscous because it is clearly observed by Testle (1987) in the case of a rigid cylinder moving towards a gas–liquid interface with zero surface tension in ideal ambient liquid. In his figure 4 an indentation under the level of the undisturbed interface is observed for the same penetration depth.

A bulge is observed in the liquid–liquid interface at the fore part of the particle at $t > 20$, followed by toroidal dimpling and a toroidal bulge – see figure 14. Similar effects have been observed in the experiments of Hartland (1968) for a rigid sphere sedimenting towards a liquid–liquid interface, and in the computations of Shopov *et al.* (1990) for a bubble approaching a spherical wall. All these results are simply explained by the influence of the additional hydrostatic pressure in the hemispherical film – see Hartland (1968).

4. Conclusions and discussion

The unsteady interaction of a fluid particle (drop or bubble) with a liquid–liquid interface for low and intermediate Reynolds number is studied in the present paper. The numerical method used allows us to investigate many inertial and transient effects which were not included in previous theories. The unsteady simulation yields information about the times of the appearance and disappearance of the hydrodynamic effects or their time stability, as well as data for the speed of the development of the processes.

A comparison of drop and interface quasi-static shapes during the coalescence at $\mathscr{R} \ll 1$ with an experiment of Hartland (1969) and with the theory of Chi & Leal (1989) is presented. The three results are in a good agreement. The results obtained for the rate and modes of film drainage are also in agreement with the conclusions of Jones & Wilson (1978) and Chi & Leal (1989).

The investigation of the intermediate-distance interaction phase shows the presence of a transient inertial concavity at the particle rear at intermediate or large Reynolds and Eötvös numbers. The amplitude of this concavity grows with the increase of these parameters. This effect is also present in the case of a rigid interface (Shopov *et al.* 1990), but is in the present case comparatively less pronounced.

The overall flattening of the particle and bulging of the interface is a typical consequence of the interaction. But bubble elongation is also observed in this stage for a small viscosity of the upper liquid, a large viscosity of the lower one and a large deformability of the liquid–liquid interface.

The sharpening of the particle edges at the end of the intermediate-distance interaction stage is a typical large-Reynolds-number, large particle deformability effect. This effect was also observed by Shopov *et al.* (1990) in the case of a rigid interface but is now clearer owing to the flexibility of the interface. After a time, when the influence of the inertia fades away, this effect diminishes.

Two different modes of the close-range interaction of the particle and the interface are studied. These are film drainage and tailing modes, established in the investigation of Geller *et al.* (1986) in the case of rigid sphere motion towards a fluid–fluid interface and observed in the experiment of Shan *et al.* (1972) in the case of passage of a drop through a liquid–liquid interface.

First, we consider the behaviour of bubbles and drops in the film drainage mode. Our results confirm the importance of the viscosity ratio $\lambda = \lambda_2$ between the upper and lower liquid for the drainage configuration. The simple rule proposed by Chi & Leal (1989) for $\mathscr{R} \ll 1 - \lambda \gg 1$ dimpling drainage, $\lambda \sim 1$ uniform thickness, $\lambda < 1$ uniform drainage – appears to be generally applicable also for finite but still modest Reynolds numbers. But obviously the other governing parameters are also important for the film shape.

We have not paid very much attention on the tailing mode, because of its relative rarity compared to film drainage, but two interesting phenomena are observed in this case: (i) a surface wave is observed at about the time of the full penetration of the particle across the initial position of the liquid–liquid interface; (ii) a ring dimpling develops at the drop front in the tailing phase for a tail length of several particle diameters.

Finally, we performed an experiment showing appearance of bubble instability in the particle–interface interaction. It takes place at relatively large Reynolds and Eötvös numbers ($\mathscr{R} \sim 100$, $\mathscr{E} \sim 25$).

We thank Professor Z. D. Zapryanov for having suggested the study of this problem and for providing continuous encouragement in the process of work. The authors wish to thank also Professor R. D. Lazarov as well as the referees of the paper for their helpful comments on the manuscript. This work was supported by Grant 55-26-3-1987 and Grant 623 of the Bulgarian Ministry of Science and Higher Education.

REFERENCES

Bach, P. & Villadsen, J. 1984 Simulation of the vertical flow of a thin, wavy film using a finite-element method. *Intl J. Heat Mass Transfer* **37**, 815–827.

Bhaga, D. & Weber, M. E. 1981 Bubbles in viscous liquids: shapes, wakes and velocities. *J. Fluid Mech.* **105**, 61–85.

Chi, B. K. & Leal, L. G. 1989 A theoretical study of the motion of a viscous drop toward a fluid interface at low Reynolds number. *J. Fluid Mech.* **201**, 123–146.

Cliffe, K. A. & Lever, D. A. 1986 A comparison of finite element methods for solving flow past a sphere. *J. Comput. Phys.* **62**, 312–330.

Clift, R., Grace, J. R. & Weber, M. E. 1978 *Bubbles, Drops and Particles.* Academic.

Dandy, D. S. & Leal, L. G. 1989 Buoyancy-driven motion of a deformable drop through a quiescent liquid at intermediate Reynolds numbers. *J. Fluid Mech.* **208**, 161–192.

Engelman, M. S., Sani, R. L., Gresho, P. M. & Bercovier, M. 1982 Consistent vs. reduced integration penalty methods for incompressible media using several old and new elements. *Intl J. Numer. Meth. Fluids* **2**, 25–42.

Geller, A. S., Lee, S. H. & Leal, L. G. 1986 The creeping motion of a spherical particle normal to a deformable interface. *J. Fluid Mech.* **169**, 27–69.

HARLOW, F. H. & SHANNON, J. P. 1967 The splash of a liquid drop. *J. Appl. Phys.* **38**, 3855–3866.

HARTLAND, S. 1967*a* The coalescence of a liquid drop at a liquid–liquid interface. Part 1. Drop shape. *Trans. Inst. Chem. Engrs* **45**, T97.

HARTLAND, S. 1967*b* The coalescence of a liquid drop at a liquid–liquid interface. Part 2. Film thickness. *Trans. Inst. Chem. Engrs* **45**, T102.

HARTLAND, S. 1967*c* The coalescence of a liquid drop at a liquid–liquid interface. Part 3. Film rupture.*Trans. Inst. Chem. Engrs* **45**, T109.

HARTLAND, S. 1968 The approach of a rigid sphere to a deformable liquid–liquid interface. *J. Colloid Sci.* **26**, 383–394.

HARTLAND, S. 1969 The effect of circulation patterns on the drainage of the film between a liquid drop and a deformable liquid–liquid interface. *Chem. Engng Sci.* **24**, 611.

JONES, A. F. & WILSON, S. D. R. 1978 The film drainage problem in drop coalescence. *J. Fluid Mech.* **87**, 263–288.

KEUNINGS, R. 1986 An algorithm for the simulation of transient viscoelastic flows with free surface. *J. Comput. Phys.* **62**, 199–220.

MACKAY, G. D. M. & MASON, S. G. 1963 The gravity approach and coalescence of fluid drops at liquid interfaces. *Can. J. Chem. Engng* **41**, 203–215.

MINEV, P. 1990 Numerical modelling of the motion of a gas bubble toward a fluid–fluid interface. *C. R. Acad. Bulg. Sci.* **43** (2), 17–20.

POZRIKIDIS, C. 1990 The instability of a moving viscous drop. *J. Fluid Mech.* **210**, 1–21.

PRINCEN, H. M. 1963 Shape of a liquid drop at a liquid–liquid interface. *J. Colloid Sci.* **18**, 178–195.

PRINCEN, H. M. & MASON, S. G. 1965 Shape of a fluid drop at a fluid–fluid interface. I. Extension and test of two-phase theory. *J. Colloid Interface Sci.* **29**, 156.

RIOLO, E., REED, X. B. & HARTLAND, S. 1975 The effect of hydrodynamic coupling on the steady drainage of a thin film between a solid sphere approaching a fluid–liquid interface. *J. Colloid Interface Sci.* **50**, 49–62.

SHAN, S. T., WASAN, D. T. & KINTNER, R. C. 1972 Passage of a liquid drop through a liquid–liquid interface. *Chem. Engng Sci.* **27**, 881–893.

SHOPOV, P. J. 1990 Numerical method for viscous free-surface hydrodynamical problems. In *Proc. Conf. on Numerical Methods for Free Boundary Problems, Jyvaskyla, Finland* (ed. P. Neittaanmaki), pp. 350–362. Birkhauser.

SHOPOV, P., MINEV, P., BAZHLEKOV, I. & ZAPRYANOV, Z. 1990 Interaction of a deformable bubble with a rigid wall at moderate Reynolds number. *J. Fluid Mech.* **219**, 241–271.

TAYLOR, T. & ACRIVOS, A. 1964 On the deformation and drag of a falling viscous drop at low Reynolds number. *J. Fluid Mech.* **18**, 466–476.

TESTLE, J. G. 1987 Inviscid flow about a cylinder rising to a free surface. *J. Fluid Mech.* **182**, 149–168.